arXiv:hep-lat/9801037v1 27 Jan 1998

COLO-HEP-396

Structure of the QCD Vacuum As Seen By Lattice Simulations

T. DeGrand, Anna Hasenfratz, Tamás Kovács
Physics Department, University of Colorado,
Boulder, CO 80309 USA

Abstract

This talk is a review of our studies of instantons and their properties as seen in our lattice simulations of $SU(2)$ gauge theory. We have measured the topological susceptibility and the size distribution of instantons in the QCD vacuum. We have also investigated the properties of quarks moving in instanton background field configurations, where the sizes and locations of the instantons are taken from simulations of the full gauge theory. By themselves, these multi-instanton configurations do not confine quarks, but they induce chiral symmetry breaking.

Talk presented by T. DeGrand at the 1997 Yukawa International Seminar
"Nonperturbative QCD–Structure of the QCD Vacuum"

1 Introduction

What features of the QCD vacuum are responsible for confinement or for the generation of the observed structure of hadron spectroscopy? This question might, in principle, be answered by lattice simulations of non-Abelian gauge theories. We have been studying the properties of instantons from $SU(2)$ lattice simulations. This talk is a survey of our work as presented in Refs. [1, 2, 3, 4, 5].

The study of the QCD vacuum using lattice Monte Carlo is complicated by two problems. The first one is that the dominant features of the QCD vacuum as seen in lattice simulations are short distance fluctuations (as they would be for any quantum field theory). They are basically uninteresting noise. The solution to this problem is to invent operators which are insensitive to the short distance behavior of the field variables. This brings the second problem: The separation of vacuum structure into short distance and long distance parts is ambiguous, and what one sees can depend strongly on the operators one uses. All direct smoothing transformations[6] distort the original lattice configuration. This makes the extraction of (continuum) short to medium distance physics, like observations of topological objects, very delicate. If any space-time symmetric smoothing transformation is repeated enough times, all the vacuum structure in any finite volume, including the simulation volume, will be washed away. Thus, it does not make sense to extrapolate one's results to the limit of a very large number of smoothing steps. The only measurements which are physically meaningful are measurements which are extrapolated back to the original lattice, that is, back to zero smoothing steps. This requires careful monitoring of observables over the whole history of smoothing transformations.

In QCD instantons may be responsible for breaking axial symmetry and resolving the $U(1)$ problem. [7] The relevant observable is the topological susceptibility χ_t, defined as the infinite volume limit of

$$\chi_t = \langle \int d^4x Q(x)Q(0)\rangle = \frac{\langle Q^2\rangle}{V} \tag{1}$$

where Q is the topological charge and V the space time volume. In QCD χ_t is a dimension-4 object with no weak coupling expansion, and a calculation of χ_t in physical units in the continuum requires nonperturbative techniques. In the large-N_c limit the mass of the η' is (probably!) related to the topological susceptibility through the Witten-Veneziano formula[8]

$$\frac{f_\pi^2}{2N_f}(m_{\eta'}^2 + m_\eta^2 - 2m_K^2) = \chi_t. \tag{2}$$

The left hand side of this equation is equal to (180 MeV)^4 in the real world.

Based on phenomenological models, it has been argued that instantons are largely responsible for chiral symmetry breaking and the low energy hadron and glueball spectrum. [9, 10] Instanton liquid models attempt to reproduce the topological content of the QCD vacuum and conclude that hadronic correlators in the instanton liquid show all the important properties of the corresponding full QCD correlators. These models appear to capture the essence of the QCD vacuum, but their derivations involve a number of uncontrolled approximations and phenomenological parameters.

Instanton physics on the lattice is as full of controversy as continuum instanton physics. There are presently three different ways of measuring a topological charge. The "geometric" definition[11, 12] reconstructs a fiber bundle from the lattice gauge field and identifies the second Chern number of this bundle with the topological charge. It will always give an integer, but if the configuration is sufficiently rough, it can fail catastrophically. "Algebraic" definitions[13] introduce some lattice discretization of Q, as a sum of closed paths of loops. The worst aspect of the algebraic definitions is that the topological charge can mix with quantum fluctuations. Finally, one can define Q through fermionic operators. (For a recent example, see Ref. [14].) All these definitions have a cutoff: they cannot see instanton (like) configurations when the instanton radius is too small (typically $\rho/a \simeq 1-2$). It is usually not possible to specify this cutoff precisely, and it can contaminate lattice measurements.

2 Finding Instantons

We have explored three different methods for extracting information about topology from lattice simulations. Each has its own strengths and weaknesses.

2.1 Inverse Blocking

"Inverse blocking" does not distort the original configuration. This technique has been introduced by Hasenfratz[15] in his lectures. Imagine beginning with a set of lattice variables $\{V\}$ on a lattice whose spacing is a and lattice size is L. The lattice action is a fixed-point (FP) action [16] $S^{FP}(U)$. The inverse blocking transformation constructs a set of fine lattice variables $\{U\}$ occupying a lattice of lattice spacing $a/2$ and lattice size $2L$, by solving the steepest-descent equation

$$S^{FP}(V) = \min_{\{U\}} \left(S^{FP}(U) + \kappa T(U,V) \right), \tag{3}$$

where $\kappa T(U,V)$ is the blocking kernel. Inverse blocking identifies the smoothest among the configurations that block back to the original configuration. Since for fixed point actions, topology is unchanged by inverse blocking, the strategy is to take a rough configuration (generated by Monte Carlo using a FP action), inverse block it, and measure the charge on the fine lattice, where the instantons are twice as big and charge measurement is more reliable. We did this[2] and found $\chi_t = (235(10)\ \text{MeV})^4$ for $SU(2)$. This created a low-level controversy, since our number was larger than other measurements.[14, 18, 19]

Inverse blocking is reliable, but it is very expensive. In four dimensions, one can only perform it once (to go from lattice spacing a to $a/2$). The fine configurations are still too rough to identify individual instantons.

2.2 Cycling

Our smoothing mechanism for seeing instantons is called "cycling." [3] One first performs an inverse blocking from a coarse lattice to a set of fine lattice variables by solving Eqn. 3. Now the original lattice occupies one of the 16 sublattices of the fine lattice. Next, we perform a blocking transformation to a set of coarse variables $\{W\}$ based on one of the other sublattices. The delicate coherence among the fine variables is broken and the new coarse variables are strongly ordered on the shortest distance scale (as measured, for example, by the expectation value of the plaquette) while retaining all long distance physics (because they are generated by a RG blocking transformation). This is the second part of the cycling transformation $V_\mu(x) \to U_\mu(x) \to W_\mu(x)$. Cycling steps can be iterated, and a few cycling steps can reduce the plaquette to within 0.001 of its free-field value.

Individual instantons can be seen after a few cycling steps. Their sizes drift with smoothing (see the next section for pictures) but the drift is small enough that we can extrapolate their properties back to zero cycling steps. We found $\chi_t^{1/4} = 230(10)$ MeV for $SU(2)$, an instanton density of about two per fm^4, and a mean instanton radius of about 0.2 fm. Again, the susceptibility is higher than others', and now the mean instanton size is smaller than other measurements, although it agrees with the predictions of the interacting instanton liquid model. [9, 10]

Cycling is still quite expensive because of the inverse blocking step. This makes it hard to push to small lattice spacing and to test scaling.

2.3 RG Mapping

Cycling produces a sequence of coarse ($\{V\}$) and fine ($\{U\}$) lattices $\{V\} \to \{U_1\} \to \{V_1\} \to \{U_2\} \to \{V_2\} \to \ldots$. RG mapping is a technique for eliminating the inverse blocking step and generating a sequence of coarse lattices $\{V\} \to \{W_1\} \to \{W_2\} \to \ldots$ where $\{W_n\}$ is an approximation to $\{V_n\}$. The idea is that, while formally the inverse blocking is non-local, for local FP actions the dependence of the fine links on the original coarse links dies away exponentially with their separation [16] and the mapping $\{V\} \to \{U_1(V)\} \to \{V_1(V)\}$ can be considered local. The $\{W_n\}$ lattice can be constructed from the original coarse $\{V\}$ lattice as a sum of loops of $\{V\}$'s which are designed to reproduce a cycled $\{V_n\}$. We discovered that this could be done by APE-smearing: [20] from a set $\{V\}$ construct a new set of links $\{X\}$ by

$$\begin{aligned} X_\mu(x) = (1-c)V_\mu(x) \quad &+ \quad c/6 \sum_{\nu \neq \mu} (V_\nu(x) V_\mu(x+\hat{\nu}) V_\mu(x+\hat{\nu})^\dagger \\ &+ \quad V_\nu(x-\hat{\nu})^\dagger V_\mu(x-\hat{\nu}) V_\mu(x-\hat{\nu}+\hat{\mu})), \end{aligned} \tag{4}$$

with $X_\mu(x)$ projected back onto $SU(2)$ to generate $W_\mu(x)$. We found that a series of steps with $c = 0.45$ was a good choice to mock up cycling.

RG-mapping is very cheap, but the price is that everything which is measured must be monitored carefully, and extrapolated (if necessary) back to zero mapping steps.

The problem is that any approximation to the fixed point charge is expected to distort the charge density profile. We have to correct this distortion. This can be done by monitoring how the charge density–measured by the FP charge–changes in the course of smoothing and extrapolating this back to zero smoothing steps. Of course we cannot directly measure the FP charge since this would involve several inverse blocking steps. However after a few smoothing steps the configurations become smooth enough so that our improved charge operator is very close to the exact FP charge and data taken after further smoothing can be used for extrapolating back.

As an example, we consider a 16^4 configuration generated with Wilson action $\beta = 2.5$. Fig. 1 shows the size of the 8 "stable" objects as a function of the APE-smearing steps. From the 4 instantons (diamonds) 3 increase in size while one decreases, but all vary linearly with smearing steps. The slope of the linear change for all of them is small. Three of the anti-instantons (bursts) behave similarly, though one has a slightly larger slope. The fourth anti-instanton (crosses) starts to grow rapidly after 18 smearing steps and will disappear after a few more steps. This object is likely to be a vacuum fluctuation, not an instanton.

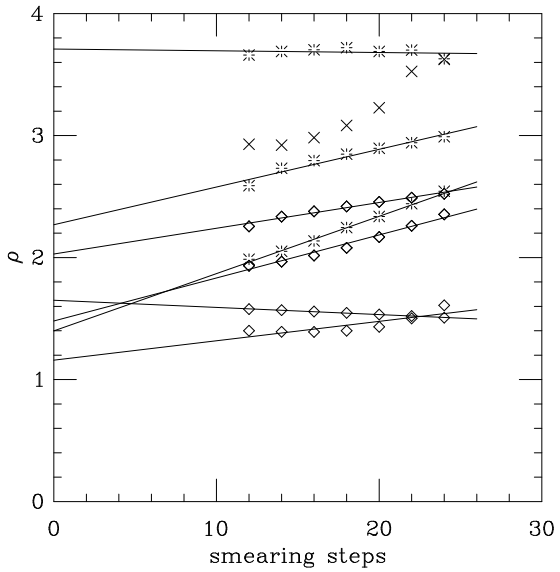

Figure 1: Radius versus APE-smearing steps of instantons (diamonds) and anti-instantons (bursts and crosses) on a 16^4 $\beta = 2.5$ configuration.

In the early stages of cycling (1-2 steps) we see many lumps of charge. Most of them quickly grow or shrink away. The locations of what we call true topological objects are stable over many smearing steps and their size changes slowly. To identify them on the lattice one has to track them over several smearing steps and monitor their behavior.

Instantons present in QCD simulations differ from hand crafted instantons in trivial background configurations in that the former usually grow while the latter objects always shrink under APE smearing.

Neither cycling nor RG-mapping affect the string tension, but the short distance part of the potential is distorted.

One of our goals was to compare results obtained with the cycling/RG mapping method with results published using other algorithms [17, 18, 19], so we used the Wilson action in conjunction with RG-mapping.

We observe, as expected, a small systematic decrease in the susceptibility as we increase the number of smearing steps. At large β the change is small and statistically insignificant. Only at $\beta = 2.4$, where the configurations are the

roughest, do the 12 and 24 smearing steps results differ by about a standard deviation.

The susceptibility increases by 10% from $\beta = 2.4$ to $\beta = 2.5$ but stabilizes after that at the value $\chi_t^{1/4} = 220(6)$ MeV. We interpret the change between the extrapolated $\beta = 2.4$ result and the larger β results as due to the absence of small instantons at $\beta = 2.4$ because of the larger lattice spacing. This interpretation will be supported by the instanton size distribution result discussed below.

We have identified individual instantons after every 2 APE-smearing steps between 12 and 24 steps. Since these configurations are still rough, many of the objects identified as instantons are in fact vacuum fluctuations and disappear after more smoothing steps. Figure 2 shows the observed instanton size distribution on the 12 and 24 times smeared lattices at $\beta = 2.5$. For comparison we also plot the result of Ref. [17] which corresponds, in our normalization, to about 100 times smeared lattices. It is obvious from the figure that the total number of identified objects decreases as we increase the smoothing. The density of identified objects is 4.6 per fm^4 after 12 smearing steps, 3.0 per fm^4 after 24 smearing steps, and about 2 per fm^4 in Ref. [17]. These density values are considerably larger than the expected value of about 1 per fm^4. The maximum of all 3 distributions is around $\bar{\rho} \approx 0.3$ fm, but that does not mean that on the original lattice $\bar{\rho} \approx 0.3$ fm since instantons usually grow under smearing. This growth can also be observed from the increasing tail of the distribution, especially after the many blocking steps of Ref. [17].

Our final result for the instanton size distribution (after extrapolation back to zero smoothing steps) is shown in Figure 3, where we overlay the data obtained at $\beta = 2.4$ (octagons on 12^4, squares on 20^4 lattices), $\beta = 2.5$ (diamonds), and $\beta = 2.6$ (bursts). Since the smoothing method cannot identify instantons with $\rho \leq 1.5a$, we chose the bins such that the second bin for each distribution starts at $\rho = 1.6a$. That means that we expect the second bin of each distribution to be universal. The first bins on the other hand contain only some of the small instantons and their value is not expected to be universal.

The four distributions form a universal curve indicating scaling. The $\beta = 2.4$ curves cover only the $\rho > 0.2$ fm region, and small instantons are obviously missing. The agreement between the 12^4 and 20^4 configurations at $\beta = 2.4$ indicate that a linear size of about 1.4 fm is sufficient to observe all the topological objects. The $\beta = 2.5$ and 2.6 distributions have most of the physically relevant instantons, supporting the scaling behavior observed for the topological susceptibility.

The instanton liquid model predicts a very similar picture to ours. In

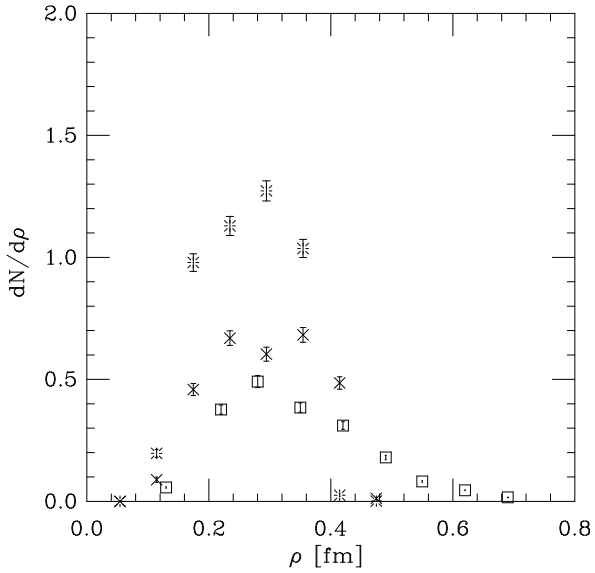

Figure 2: The size distribution on 12 (bursts) and 24 (crosses) times APE smeared lattices at $\beta = 2.5$. The square symbols are the results of Ref. 11 rescaled appropriately.

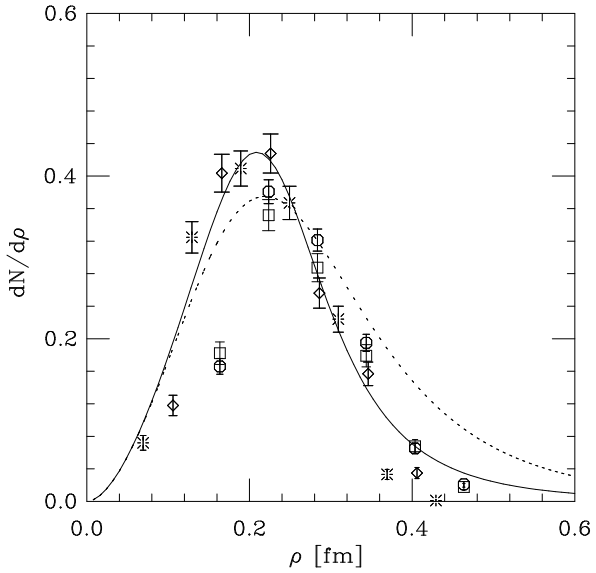

Figure 3: The size distribution of instantons. Octagons correspond to $\beta = 2.4$ 12^4, squares to $\beta = 2.4$ 20^4, diamonds to $\beta = 2.5$ and bursts to $\beta = 2.6$. The first bin of each distribution is contaminated by the cut-off. The solid curve is a two parameter fit to the data points according to the formula in Ref. 23. The dashed curve is a similar fit from Ref. 23 which describes the instanton liquid model quite closely.

Ref. [21] Shuryak predicted an instanton size distribution that peaked around $\rho = 0.2$ fm. The curve in Fig. 3 is a fit using the two loop perturbative instanton distribution formula with a "regularized" log

$$S_I = \frac{8\pi^2}{g^2(\rho)} = b_0 L + b_1 \log L \tag{5}$$

$$L = \frac{1}{p} \log[(\rho\Lambda_{inst})^{-p} + C^p] \tag{6}$$

where b_0 and b_1 are related to the first two coefficients of the perturbative β function and p and C are arbitrary parameters. The solid curve is a fit to our data while the dashed curve is the fit given in Ref. [21] which describes the instanton liquid model quite closely. The difference between the two fits is significant at large ρ values only. We do not know if changing the parameters of the interacting instanton liquid model slightly would change the predictions of that model improving the agreement with the Monte Carlo data.

To make a long story short, we believe that there are two reasons why our instanton numbers are different from those of Refs. [17, 18, 19]. First, we are sensitive to instantons of smaller radius. As we cut larger and larger instantons from our sample, we see χ_t fall. Second (and most important) we extrapolate our measurements back to zero smoothing steps. Instantons generally grow under smoothing, so our extrapolated sizes are smaller.

3 What Do Instantons Do?

To test what role instantons play in the QCD vacuum, we took a set of $SU(2)$ configurations with lattice spacing $a \simeq 0.14$ fm and smoothed them enough to identify the instantons. These smoothed configurations have essentially the same string tension as the original configurations, even though about seventy per cent of their vacuum action is carried by the instantons. We then identified the sizes and locations of the instantons in the configurations and built multi-instanton configurations from them. We built both "parallel" and randomly oriented instanton configurations.

Notice that the instanton locations are not random, and the sizes are not taken from a model distribution–they come from the (lattice) QCD vacuum.

In Fig. 4 the heavy-quark potentials obtained from the three ensembles are compared. We can conclude that neither the parallel nor the randomly oriented instantons confine. It seems that instantons by themselves are not responsible for confinement.

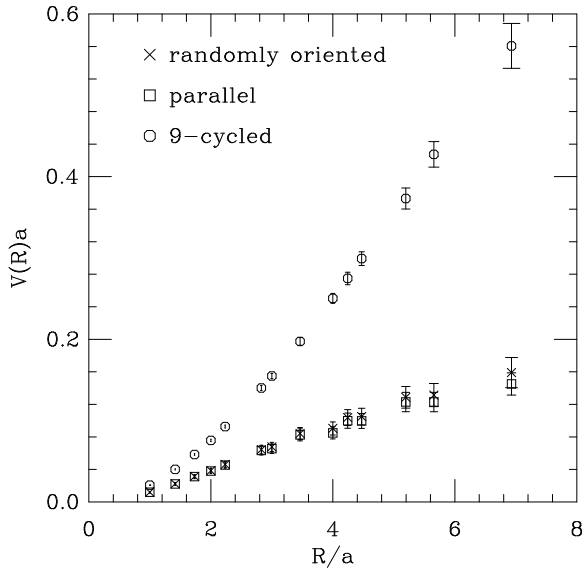

Figure 4: The heavy-quark potential measured on the 9 times cycled real configurations (octogons), the randomly (crosses) and the parallel (squares) oriented instantons.

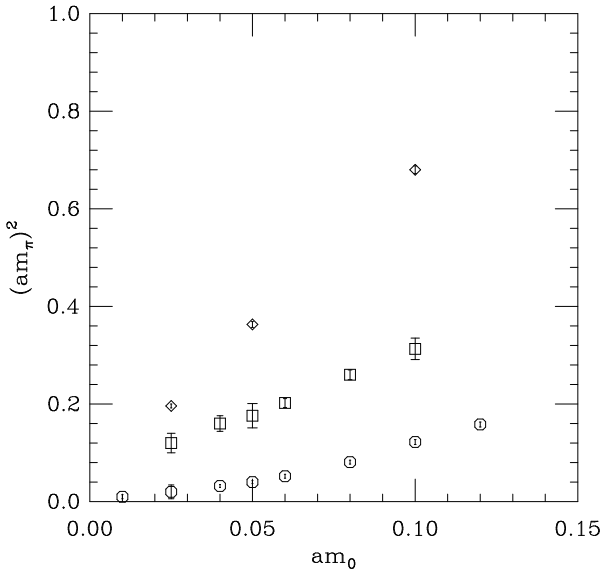

Figure 5: $(am_\pi)^2$ vs. m_0 the bare quark mass for the staggered action, with raw gauge links (diamonds) and 9-cycled links (squares). The lightest mass in the pseudoscalar channel with instanton background configurations is shown by octagons.

Next, we computed hadron spectroscopy in these background configurations. One could think of spectroscopy on the smoothed configurations as spectroscopy computed with a new kind of quark action, one which is insensitive to the short distance behavior of the gauge field. This is similar in spirit to the use of "fat links" by the MILC collaboration [22] and by J.-F. Lagaë and D. K. Sinclair [23], or of the approximate FP actions developed by one of us.[24]

Staggered fermions provide the most interesting results. It appears that cycling does not affect the ρ mass vs the Goldstone pion. However, on the smoothed lattices the non-Goldstone partner of the pion is degenerate with the pion within observational uncertainty. On the original lattices the two mesons have a mass ratio of about 1.4.

The purpose of this exercise is not to test spectroscopy in detail. The important point is that the action of the many-times-cycled configurations is dominated by instantons, and yet the asymptotic heavy quark potential and hadron spectroscopy are basically unchanged from what we saw on untouched configurations.

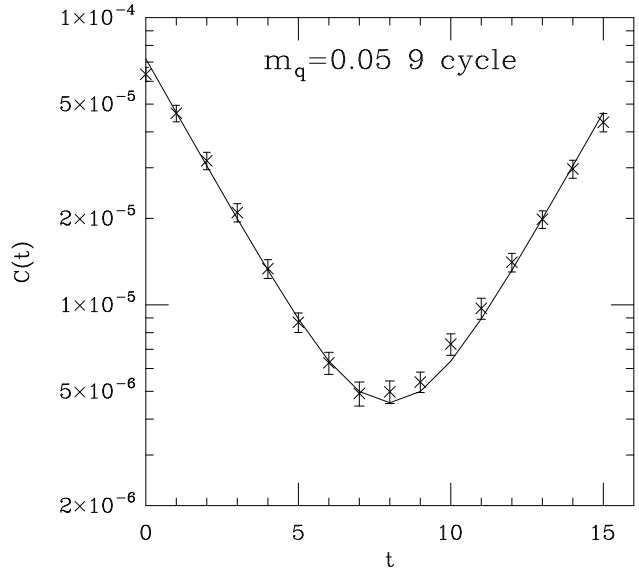

Figure 6: The pseudoscalar propagator from 9-cycled configurations, with staggered fermions of bare mass $am_0 = 0.05$.

But these results do not answer the question: Are instantons responsible for long distance physics, or are the structures responsible for long distance physics some other objects carrying low action, which have been preserved by the smoothing transformation?

We computed spectroscopy on the two types of multi-instanton ensembles using both staggered and Wilson fermions. The dominant feature of both spectroscopy calculation is that the quarks are deconfined. This is seen most easily in the staggered fermion spectroscopy.

Consider the pseudoscalar propagator of the 9-cycled configurations, shown for one quark mass in Fig. 6. It looks like any generic lattice pseudoscalar, a more-or-less pure hyperbolic cosine with no oscillations. The staggered fermion pseudoscalar propagators on instanton background fields are quite different: they show the characteristic sawtooth pattern of free antiperiodic fermions. (See Fig. 7).

Fig. 8 shows the lattice $\langle\bar{\psi}\psi\rangle$ for staggered fermions on the 9-cycled and in instanton background configurations. $\langle\bar{\psi}\psi\rangle$ in the instanton background tracks the value of $\langle\bar{\psi}\psi\rangle$ measured on the 9-cycled configurations quite closely, down to

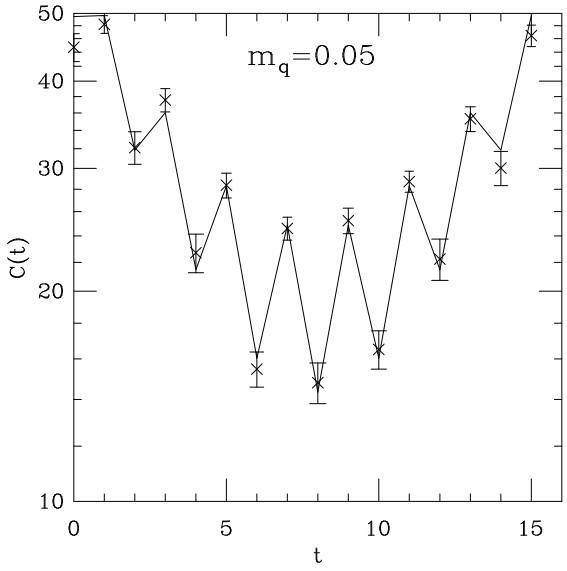

Figure 7: The pseudoscalar propagator in (randomly rotated) instanton background configurations, with staggered fermions of bare mass $am_0 = 0.05$. The curve is a fit to a single propagating particle plus the $q\bar{q}$ branch cut.

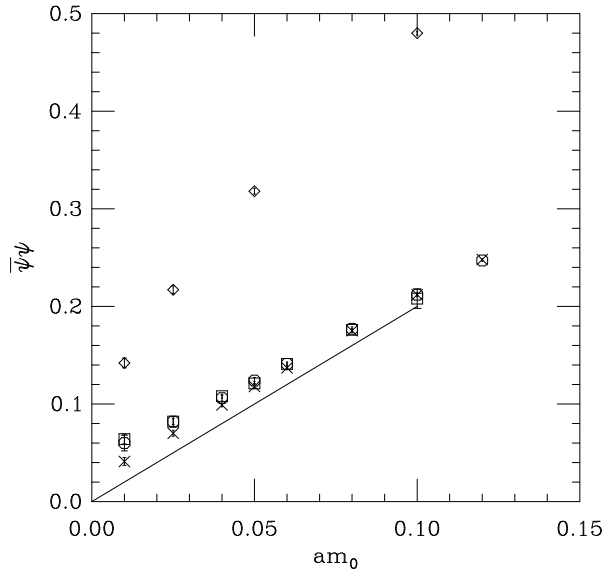

Figure 8: $\langle\bar{\psi}\psi\rangle$ from raw configurations (diamonds), 9-cycled configurations (squares), and instanton-background configurations which are parallel (crosses) and randomly oriented (octagons), vs. bare quark mass am_0. The line shows the free-field value, $2m_0$.

small quark mass. It appears that the instantons, present in equilibrium gauge field configurations of the QCD vacuum generated by Monte Carlo, are breaking chiral symmetry by themselves. This effect is a cornerstone of instanton-liquid models of hadron structure.

If $\langle\bar{\psi}\psi\rangle$ is nonzero, one expects the spectrum contains a would-be Goldstone boson (the pion) in addition to massive quarks and (possibly) other resonances. To test this hypothesis, we fit the pseudoscalar correlator to two terms: a pure hyperbolic cosine (a pole in the frequency plane), plus a $q\bar{q}$ branch cut, with the quark mass as a parameter. We used the analytic expression for the branch cut (expressed as a momentum and frequency mode sum), with the appropriate boundary conditions and source used in the simulations. In the random instanton background, we clearly see a light mass which decreases towards zero as the quark mass vanishes. (See Fig. 5.)

The quark mass in the randomly oriented instanton background is also determined by the fit. It is close to the bare mass and is less than half the rho mass–and less than half the pion mass– (as measured on the smoothed lattices).

Are there other bound states? Only for the randomly rotated instanton configurations could we see a convincing pseudoscalar, and so we restricted our analysis to that data set. We again attempted to fit to a single resonance plus a $q\bar{q}$ continuum. Of course, this assumption is questionable. The fits are not of high quality and our results should not be taken too seriously: In the "SC" channel (saturated by the π_2 and scalar mesons in the confined phase) we saw a light bound state whose mass roughly tracked the mass of the (presumed) pion resonance in the pseudoscalar channel. (That is, there is a multiplet of Goldstone bosons.) In the vector channels, a state with a mass 750-850 MeV appears, in addition to the free $q\bar{q}$ continuum. This state has about the same mass as the vector meson in the confined system. However, the dominant feature of all these channels is still the free $q\bar{q}$ continuum, with fitted quark masses of 100 MeV or lower whose energy is always lower than the mass of any (presumed) resonance.

The reader should be aware that the lattice spacing is large enough that it could contaminate the coupling of quarks to instantons.

4 Conclusions

We have measured the instanton content of the $SU(2)$ lattice vacuum. Instantons do not confine, but they seem to be connected to chiral symmetry breaking. We are presently using RG-mapping to study the properties of instantons in $SU(3)$, both in the pure gauge theory and for full QCD. This spring we expect to begin computing hadron spectroscopy in smoothed configurations and in multi-instanton background configurations. How similar will they be?

Acknowledgements

T. D. would like to thank the organizers of YKIS 97 for putting together such a diverse and interesting meeting, and for their hospitality in Kyoto. This work was supported by the U.S. Department of Energy.

References

[1] T. DeGrand, A. Hasenfratz, D. Zhu, Nucl. Phys. **B475** (1996) 321.

[2] T. DeGrand, A. Hasenfratz, D. Zhu, Nucl. Phys. **B478** (1996) 349.

[3] T. DeGrand, A. Hasenfratz,T. Kovács, Nucl. Phys. **B505** (1997) 417.

[4] T. DeGrand, A. Hasenfratz,T. Kovács, hep-lat/9711032.

[5] T. DeGrand, A. Hasenfratz, T. Kovács, hep-lat/9710078.

[6] D. J. R. Pugh, M. Teper, Phys. Lett. **B218** (1989) 326.

[7] S. Weinberg, Phys. Rev. **D11** (1975) 3583; G. t'Hooft, Phys. Rev. **D14** (1976) 3432; Phys. Rev. Lett. **37** (1976) 8.

[8] E. Witten, Nucl. Phys. **B156** (1979) 269; G. Veneziano, Nucl. Phys. **B159** (1979) 213.

[9] D. Diakanov, Lectures at the Enrico Fermi School in Physics, Varenna, 1995, hep-ph/9602375.

[10] T. Schäfer and E. V. Shuryak, "Instantons in QCD," hep-ph/9610451.

[11] B. Berg, M. Lüscher, Nucl. Phys. **B190** (1981) 412.

[12] M. Lüscher, Comm. Math. Phys. **85** (1982) 29; A. Phillips and D. Stone, Comm. Math. Phys. **103** (1986) 599. E. M. Ilgenfritz, M. L. Laursen, M. Müller-Preussker, G. Schierholz and M. Schiller, Nucl. Phys. **B268** (1986) 693; A. S. Kronfeld, M. L. Laursen, G. Schierholz, and U. J. Wiese, Nucl. Phys. **B292** (1987) 330.

[13] P. di Veccia, K. Fabricius, G. C. Rossi and G. Veneziano, Nucl. Phys. **B192** (1981) 392; Phys. Lett. **108B** (1982) 323.

[14] R. Narayanan and H. Neuberger, Nucl. Phys. **B412** (1994) 574; R. Narayanan, and P. Vranas, preprint UW-PT-97-04 and hep-lat/9702005.

[15] P. Hasenfratz, in these Proceedings.

[16] P. Hasenfratz and F. Niedermayer, Nucl. Phys. **B414** (1994) 785; T. DeGrand,A. Hasenfratz, P. Hasenfratz, F. Niedermayer, Nucl. Phys. **B454** (1995) 587, Nucl. Phys. **B454** (1995) 615.

[17] C. Michael and P.S. Spencer, Phys. Rev. **D52** (1995) 4691.

[18] Ph. de Forcrand, M. Garcia Perez and I.-O. Stamatescu, hep-lat/9701012.

[19] B. Alles, M. D'Elia, and A. Di Giacomo, hep-lat/9706016.

[20] M. Falcioni, M. Paciello, G. Parisi, B. Taglienti, Nucl. Phys. **B251[FS13]** (1985) 624. M. Albanese, et al., Phys. Lett. **192B** (1987) 163.

[21] E. V. Shuryak, Phys. Rev. **D52** (1995) 5730; Nucl. Phys. **B302** (1988) 574.

[22] MILC collaboration, hep-lat/9609036.

[23] J.-F. Lagaë and D. K. Sinclair, talk presented at Lattice '97, hep-lat/9709035.

[24] T. DeGrand, poster presented at Lattice 97, hep-lat/9709052.